frontiers | Frontiers in Pharmacology

TYPE Original Research
PUBLISHED 03 November 2022
DOI 10.3389/fphar.2022.989169

OPEN ACCESS

EDITED BY
Ramaswamy Krishnan,
Beth Israel Deaconess Medical Center,
Harvard Medical School, United States

REVIEWED BY
Erzsébet Bartolák-Suki,
Boston University, United States
Matthew Lech,
Pfizer, United States

*CORRESPONDENCE
Janette K. Burgess,
j.k.burgess@umcg.nl

SPECIALTY SECTION
This article was submitted to Respiratory Pharmacology, a section of the journal Frontiers in Pharmacology

RECEIVED 08 July 2022
ACCEPTED 24 October 2022
PUBLISHED 03 November 2022

CITATION
Blokland KEC, Nizamoglu M, Habibie H, Borghuis T, Schuliga M, Melgert BN, Knight DA, Brandsma C-A, Pouwels SD and Burgess JK (2022), Substrate stiffness engineered to replicate disease conditions influence senescence and fibrotic responses in primary lung fibroblasts.
Front. Pharmacol. 13:989169.
doi: 10.3389/fphar.2022.989169

Substrate stiffness engineered to replicate disease conditions influence senescence and fibrotic responses in primary lung fibroblasts

Kaj E. C. Blokland[1,2,3,4], Mehmet Nizamoglu[1,2], Habibie Habibie[2,5,6], Theo Borghuis[1,2], Michael Schuliga[3], Barbro N. Melgert[1,2,5], Darryl A. Knight[3,4,7], Corry-Anke Brandsma[1,2], Simon D. Pouwels[1,2,8] and Janette K. Burgess[1,2]*

[1]University of Groningen, University Medical Center Groningen, Department of Pathology and Medical Biology, Groningen, Netherlands, [2]University of Groningen, University Medical Center Groningen, Groningen Research Institute for Asthma and COPD, Groningen, Netherlands, [3]University of Newcastle, School of Biomedical Sciences and Pharmacy, Callaghan, NSW, Australia, [4]National Health and Medical Research Council Centre of Research Excellence in Pulmonary Fibrosis, Sydney, NSW, Australia, [5]University of Groningen, Department of Molecular Pharmacology, Groningen Research Institute of Pharmacy, Groningen, Netherlands, [6]Hasanuddin University, Faculty of Pharmacy, Makassar, Indonesia, [7]Providence Health Care Research Institute, Vancouver, BC, Canada, [8]University of Groningen, University Medical Center Groningen, Department of Pulmonology, Groningen, Netherlands

In fibrosis remodelling of ECM leads to changes in composition and stiffness. Such changes can have a major impact on cell functions including proliferation, secretory profile and differentiation. Several studies have reported that fibrosis is characterised by increased senescence and accumulating evidence suggests that changes to the ECM including altered composition and increased stiffness may contribute to premature cellular senescence. This study investigated if increased stiffness could modulate markers of senescence and/or fibrosis in primary human lung fibroblasts. Using hydrogels representing stiffnesses that fall within healthy and fibrotic ranges, we cultured primary fibroblasts from non-diseased lung tissue on top of these hydrogels for up to 7 days before assessing senescence and fibrosis markers. Fibroblasts cultured on stiffer (±15 kPa) hydrogels showed higher Yes-associated protein-1 (YAP) nuclear translocation compared to soft hydrogels. When looking at senescence-associated proteins we also found higher secretion of receptor activator of nuclear factor kappa-B ligand (RANKL) but no change in transforming growth factor-β1 (TGF-β1) or connective tissue growth factor (CTGF) expression and higher decorin protein deposition on stiffer matrices. With respect to genes associated with fibrosis, fibroblasts on stiffer hydrogels compared to soft had higher expression of smooth muscle alpha (α)-2 actin (*ACTA2*), *collagen (COL) 1A1* and *fibulin-1* (Fbln1) and higher Fbln1 protein deposition after 7 days. Our results show that exposure of lung fibroblasts to fibrotic stiffness activates genes and secreted factors that are part of fibrotic

responses and part of the Senescence-associated secretory phenotype (SASP). This overlap may contribute to the creation of a feedback loop whereby fibroblasts create a perpetuating cycle reinforcing progression of a fibrotic response.

KEYWORDS

cellular senescence, stiffness, GelMA hydrogels, fibrosis, SASP

1 Introduction

The extracellular matrix (ECM) is a complex structure composed of various proteins, proteoglycans and other biological factors that are secreted and/or modified by cells embedded within this microenvironment (Bonnans et al., 2014). Our understanding of ECM has greatly advanced in the last decade, particularly with respect to its role in providing essential biochemical and biomechanical cues that regulate cellular functions (Hansen et al., 2015; Zhou et al., 2018). During normal tissue homeostasis, fibroblasts that reside in the ECM are maintained in a quiescent state; meaning they do not proliferate but secrete, sustain, and remodel the ECM. The biomechanical cues provided by the three-dimensional ECM, that provides the microenvironment in which these cells reside, regulate cellular processes such as adhesion, migration, proliferation, and differentiation (Liu et al., 2010; Huang et al., 2012). Using specific receptors, including integrins, fibroblasts are able to sense and respond to changes in the ECM (Sapir and Tzlil, 2017). The mechanical forces that are generated in response to changes in the ECM local environment generate signals within the cell that rapidly propagate and activate signalling pathways (Tschumperlin et al., 2018).

The remodelling of ECM during fibrosis leads to a change in composition, structural organisation, increased crosslinking, and ultimately increased stiffness. The stiffness of healthy tissue does not exceed 5 kPa while in fibrotic tissue, the stiffness can be up to 30 times stiffer. The range of fibrotic stiffness varies depending on location and it has been reported that locally tissue can be as stiff as 20–100 kPa while the average stiffness is approximately 17 kPa (Foucher et al., 2006; Liu et al., 2010; Booth et al., 2012; Hinz, 2012; Petzold et al., 2019; de Hilster et al., 2020; Leong et al., 2021). These changes greatly influence the biochemical and biomechanical properties of the ECM, leading to alterations in cellular response such as migration and proliferation (Blokland et al., 2020a). Tissue damage that leads to disruption of mechanical homeostasis drives mechano-activation of quiescent fibroblasts into myofibroblasts, which is a feature of tissue wound repair (Humphrey et al., 2014). After successful wound repair myofibroblasts are cleared from the tissue *via* apoptosis to prevent excessive ECM production and contraction (Li and Wang, 2011). Myofibroblasts are characterised by expression of contractile proteins such as α-smooth muscle actin (αSMA) and their ability to contract tissue. During repair they play a key role in remodelling the injured tissue and are responsible for excessive ECM deposition in fibrotic diseases such as idiopathic pulmonary fibrosis (IPF). Furthermore, as a direct effect of increased matrix stiffness, fibroblasts will produce and secrete transforming growth factor (TGF)-β1, a key fibrogenic mediator (Piersma et al., 2015a; Piersma et al., 2015b). The increased stiffness and secretion of cytokines reinforce the activation which results in myofibroblast activation and progression of fibrosis creating a perpetuating feedback loop (Yan et al., 2018).

Cells that undergo (premature) cellular senescence show marked changes in morphology, phenotype, and metabolism. Most notably, irreversible cell-cycle arrest and apoptosis resistance are defining features of cellular senescence. Senescent cells remain metabolically active and acquire a dynamic pro-inflammatory secretory profile known as the Senescence-Associated Secretory Phenotype (SASP) (Coppe et al., 2010). The SASP is comprised of differently secreted pro-inflammatory and pro-fibrotic cytokines which impact on neighbouring cells and the local microenvironment (Blokland et al., 2020b). To which degree altered ECM contributes to fibrosis progression is not yet fully understood, specifically in relation to cellular senescence. Evidence is emerging that increased tissue stiffness might contribute to cellular senescence. Recently it was described that stiffness could lead to increase ROS productions which is linked to cellular senescence *via* activation of STAT3 (Waters et al., 2019; Wang et al., 2021). In addition, pathological stiffness leads to upregulation of TGF-β1, lysyl oxidase (LOX) and downregulation of micro-RNA-29 together with increased deposition of matricellular proteins they could potentially regulate cell-cycle arrest, apoptosis, and production of cytokines through the SASP (Blokland et al., 2020a). Increased ECM stiffness may drive excessive ECM production creating a perpetuating feedback loop in favour of disease progression. We hypothesised that the increased stiffness of fibrotic ECM detrimentally influences fibroblast function to perpetuate disease progression in fibrosis. Here we aimed to investigate whether adjusting the stiffness of *in vitro* produced methacrylated-gelatine (GelMA) hydrogels resembling the stiffness of healthy and fibrotic tissues could

modulate cellular senescence, the SASP or the fibrotic response in primary human lung fibroblasts.

2 Materials and methods

2.1 Methacrylated-gelatine synthesis

Gelatine was functionalised as described before with small modifications to the original protocol (Shirahama et al., 2016). Ten grams medical grade 262 Bloom Type A gelatine (Gelita, Ter Apelkanaal, the Netherlands) was added to 1 L 0.25 M carbonate-bicarbonate (CB, Sigma-Aldrich, Zwijndrecht, the Netherlands) buffer pH 9.0 and allowed to dissolve at 50°C for 60 min. Heating was turned off and then 563 µL methacrylic anhydride (MAA; Sigma-Aldrich, CCID: 12974) was added dropwise in three steps. Ten minutes after each step the pH was measured and corrected using a 3 M NaOH (Sigma-Aldrich, CCID: 14798) solution to maintain pH 9.0. The gelatine-MAA solution was allowed to react overnight at room temperature (RT) while stirring. The next day the GelMA solution was dialysed using dialysis with molecular weight cut-off of 12–14 kDa (Sigma-Aldrich) for up to 5 days against deionised water pH 9.0. After dialysis, GelMA solution was aliquoted in 50 ml tubes, frozen with liquid nitrogen and lyophilised on a Labconco Freezone 2.5 L benchtop freeze-dryer (Labconco, Kansas City, MO, United States). Samples were considered dry when weights of the tubes were stable. Three batches were produced, lyophilised, re-dissolved into one large batch and then lyophilised again to minimise batch-to-batch variation.

2.2 Trinitrobenzenesulfonic acid assay

The degree of modification of GelMA was measured using a Trinitrobenzenesulfonic acid (TNBS) colorimetric assay (Ravichandran et al., 2016). Two mg of dry GelMA and gelatine were dissolved in 1 ml of 4% w/v sodium bicarbonate solution (Sigma-Aldrich) and 1 ml of 0.5% w/v TNBS solution (Sigma-Aldrich, CCID:11045) followed by incubation at 40°C with mild shaking for 2 h. Afterwards, the solution was transferred to a 7.5 ml glass bottle and 3 ml 6N HCL solution (Sigma-Aldrich, CCID: 313) was added to stop the reaction. Unreacted TNBS was extracted twice with diethyl ether (Sigma-Aldrich, CCID: 3283) by removing the upper phase. Absorbance (346 nm) of samples was measured using a Benchmark plus UV-VIS spectrophotometer (Bio-Rad Technologies). A blank sample was generated as described above but without the addition of GelMA or gelatine and was subtracted from each measurement. The degree of functionalisation (%DoF) was calculated using the formula:

$$[\ (\text{AbsGelatine} - \text{AbsGelMA})\ /\ \text{AbsGelatine}\ ] \times 100\%$$

2.3 Fabrication of GelMA hydrogels

GelMA samples were dissolved at 5 and 8% w/v in PBS containing 1% w/v filter sterilised lithium phenyl-2,4,6-trimethylbenzoylphosphinate (LAP; TCI Europe, Zwijndrecht, Belgium, CCID: 68384915), and kept in the dark at 37 °C prior to usage. To assemble the gels, 400 µl of 5 or 8% GelMA solution was added per well of a 24-well plate (Corning, New York, United States) and irradiated using a Unic nail dryer (MEANAIL© Paris, France) equipped with a UV/VIS (405 nm) LED lamp for 4 min at 20 mW/cm^2. After irradiation, gels were allowed to swell overnight in low glucose Dulbecco's Modified Eagle Medium (DMEM) (Lonza, Geleen, the Netherlands) supplemented with 10% foetal bovine serum (FBS) (Sigma-Aldrich), 100U/mL penicillin and 100 µg/ml streptomycin (Gibco, Breda, the Netherlands), and 1% GlutaMAX (Gibco) prior to use in experiments. This media was referred to as complete growth media.

2.4 Mechanical testing with low load compression testing

Mechanical properties of the GelMA hydrogels were measured using Low Load Compression Testing (LLCT) as previously described (de Hilster et al., 2020). LLCT analyses were performed on three different locations (2.5 mm apart) of each hydrogel with a 20% fixed strain rate. The stress and strain values for each measurement were determined using formulas (i) and (ii), respectively. Young's modulus (E, i.e., stiffness) values were calculated from the slope of the linear region of the Stress-Strain graph, using formula (iii). After the peak value, the viscoelastic relaxation measurement was performed for 5 s, and the relaxation percentage was measured according to the formula (iv).

$$Stress = \frac{Load\ x\ g}{Area} \quad \text{(i)}$$

$$Strain = \frac{Deformation}{Thickness} \quad \text{(ii)}$$

$$E(t) = \frac{Stress}{Strain} \quad \text{(iii)}$$

$$Relaxation\ (t) = \frac{E(t_0) - E(t)}{E(t_0)} \quad \text{(iv)}$$

2.5 Human lung tissue

The study protocol was consistent with the Research Code of the University Medical Centre Groningen (https://www.umcg.nl/SiteCollectionDocuments/English/Researchcode/umcg-research-code-2018-en.pdf) and national ethical and professional guidelines ("Human tissue and medical research: code of conduct

TABLE 1 Characteristics of fibroblast donors.

Donor #	Sex	Age	Smoking history	Pack years	FEV1/FVC
1	F	49	Current	33	82.3
2	F	50	Never	0	77.9
3	F	47	Current	30	73.9
4	F	51	Current	70	78.3
5	F	49	Ex	35	77.7
6	F	46	Ex	32	81.5
7	M	69	Current	20	70.0

F = female, M = male and Ex = former smoker.

for responsible use (2011)", https://www.coreon.org/wp-content/uploads/2020/04/coreon-code-of-conduct-english.pdf). Lung fibroblasts and lung tissues used in this study were derived from leftover lung material after lung surgery and transplant procedures. This material was not subject to the Medical Research Human Subjects Act in the Netherlands, and, therefore, an ethics waiver was provided by the Medical Ethical Committee of the University Medical Center Groningen (UMCG). All samples and clinical information were deidentified before experiments were performed. Fibroblasts were isolated from macroscopically and histologically normal tissue as described before (Noordhoek et al., 2005).

Table 1 shows the characteristics of fibroblast donors used in this study: comprising 6 female and 1 male donors, 4 current smokers, 2 ex-smoker and 1 never smoker. The average age of the donors was 51.6 ± 7.87 years, all of which had normal lung capacity as demonstrated by a forced expiratory volume in 1 s/forced vital capacity (FEV1/FVC) that was above 70%.

2.6 Cell culture

Primary LFs were cultured in complete growth media and used between passage 3 to 5 (Blokland et al., 2020b). LFs were routinely checked for *mycoplasma* infection using a PCR assay, and only used when certified negative (Uphoff and Drexler, 2002). To improve attachment of fibroblasts, hydrogels were coated with a 5% w/v Bovine Serum Albumin (BSA) solution (Sigma-Aldrich) in low glucose DMEM for 24 h prior to cell seeding. Twenty thousand LFs/gel were seeded on top of soft and stiff GelMA hydrogels in complete growth media. After 24 h, the media was replaced with fresh complete growth media, and cells were allowed to grow for another 6 days after which supernatant, RNA, hydrogels for live/dead stain and immunofluorescent staining were harvested. Supernatants were collected, pooled, and centrifuged for 5 min at 300 x g to remove debris and dead cells after which the cell-free supernatants were stored at -80 °C. Hydrogels in RNA lysis buffer (Machery-Nagel, Düren, Germany) were stored at −80°C until RNA isolation. Hydrogels for immunofluorescent imaging were fixed in 2% paraformaldehyde (PFA; Sigma-Aldrich) and 0.2% glutaraldehyde in PBS for 30 min. The hydrogels were then washed three times in PBS and stored in PBS supplemented with 1% Pen/Strep at 4°C until analyses.

2.7 Live and dead cell assays

Cell viability after 1 and 7 days was examined using Calcein AM (Thermo Scientific, Breda, the Netherlands, CCID: 390986) for live cells and propidium iodide (PI; Sigma-Aldrich, CCID: 104981) for dead cells. Briefly, GelMA hydrogels were washed and incubated with Hank's Balanced Salt Solution (HBSS; Gibco) containing magnesium and calcium for 20 min at 37°C. A working solution was prepared containing 5 μM Calcein AM and 2 μM PI in HBSS, which was added to the GelMA hydrogels before they were incubated for 20 min in the dark. Images were captured using a EVOS Cell Imaging System (Thermo Scientific). ImageJ was used to create an overlay of both GFP and Texas Red channels without modifications (Schneider et al., 2012). Morphological analysis was performed using CellProfiler software (Broad Institute, MIT, Cambridge MA) (Stirling et al., 2021).

2.8 Gene expression analysis

Total RNA from GelMA hydrogels was isolated using a Nucleospin RNA isolation kit (Machery-Nagel). Media was removed and lysis buffer in a 1:3.3 sample-to-buffer ratio was added to each well before incubation for 15 min on ice, after which the samples (gel and lysis buffer) were stored at -80 °C. Samples were thawed on ice and mixed thoroughly before the lysis buffer was transferred to a new Eppendorf tube without the GelMA hydrogel. RNA isolation was performed according to the manufacturer's instructions. Total RNA was quantified using the Qubit HS RNA assay kit (Thermo Scientific)

TABLE 2 Primers and probes with designated exon boundaries.

Gene	Number	Exon boundary
18S	Hs99999901_s1	1-1
CDKN2A	Hs00923894_m1	2-3
CDKN1A	Hs00355782_m1	2-3
P53	Hs01034249_m1	10-11
IL-6	Hs00174131_m1	4-5
CXCL8	Hs00174103_m1	1-2
DCN	Hs00370385_m1	7-8
ACTA2	Hs00426835_g1	2-3
COL1A1	Hs00164004_m1	1-2
FN1	Hs01549976_m1	8-9
FBLN1	Hs00242545_m1	13-14
FBLN1C	Hs00242546_m1	14-15
LOX	Hs00942483_m1	5-6
TGF-β1	Hs00998133_m1	6-7
CTGF	Hs00170014_m1	4-5

18S ribosomal RNA, 18S, Cyclin-dependent kinase inhibitor 2A = CDKN2A, Interleukin 6 = IL-6, Chemokine ligand 8 = CXCL8, Decorin = DCN, Actin alpha 2 = ACTA2, Collagen 1α1 = COL1A1, Fibronectin = FN1, Fibulin-1 = FBLN1, Lysyl oxidase = LOX, Transforming growth factor β1 = TGF-β1, Connective tissue growth factor = CTGF.

according to the manufacturer's instructions. RNA was reversed transcribed into cDNA using the ReverseAid First Strand cDNA Synthesis Kit (Thermo Scientific). DNA was amplified using GoTaq Probe qPCR Master Mix (Promega, Leiden, the Netherlands) and TaqMan Gene Expression Assay (Thermo Scientific) on a ViiA7 Real-Time PCR System (Applied Biosystems, Breda, the Netherlands) with the relevant predeveloped primers listed in table 2 (Thermo Scientific).

2.9 Immunofluorescence

For immunofluorescence cells were washed twice with PBS and fixed with 2% PFA/0.2% glutaraldehyde (Sigma-Aldrich) in PBS for 20 min at room temperature. Fixed cells were permeabilized with 0.5% Triton X-100 in PBS for 10 min and incubated with 2.2% bovine serum albumin (BSA) for 30 min. Next cells were incubated with primary antibodies for 16 h: rabbit polyclonal to YAP (GeneTex Cat# GTX129151, 0.3 μg/ml, RRID:AB_2885910), mouse monoclonal to P16 (Abcam Cat# ab54210, 2.5 μg/ml, RRID:AB_881819), rabbit polyclonal to Decorin (Proteintech Cat# 14667-1-AP, 0.9 μg/ml, RRID:AB_2090265) 14667-1-AP; ThermoFisher), rabbit polyclonal to fibulin-1 (Thermo Fisher Scientific Cat# PA5-103841, 3.33 μg/ml, RRID: AB_2853174) in PBS +0.1% Triton X-100 and 2.2% BSA. After three washes with PBS containing 0.5% Tween-20 samples were incubated with fluorescent labelled secondary antibodies containing 4′,6-diamidino-2-phenylindole (DAPI; Roche Cat# 10236276001, 1.0 μg/ml) for 30 min. Actin was visualized by incubating with TRITC labelled-Phalloidin (Sigma-Aldrich Cat# P1951, 100nM, RRID:AB_2315148) in PBS for 30 min. Slides were mounted in Citifluor (Agar Scientific, Stansted, United Kingdom). Fluorescent photomicrographs were acquired using a SP8 scanning confocal microscope equipped with photomultiplier tubes (PMTs) (Leica Microsystems, Amsterdam, Netherlands) and a HC PL APO CS2 63x/1.4 oil immersion objective at room temperature. Fluorescent images were loaded in ImageJ and subsequently split into the separate channels. The DAPI channel was used to count the number of nuclei and determine the nucleic area. This was done using the particle Analyzer with particles size set at 50—Infinity. Then, a mask was made of the nuclear area. In the YAP channel total positive area was measured and by using the nuclear mask also the nuclear area was determined. The nuclear fraction was calculated as follows: total nuclear YAP was divided by total YAP to calculate the ratio between total and nuclear YAP. Matrix ECM patterns were analysed using The Workflow Of Matrix BioLogy Informatics (TWOMBLI) as described before (Wershof et al., 2021).

2.10 Enzyme linked immunosorbent assay

Secreted IL-6 (DY205), CXCL8 (DY208), DCN (DY143), TGF-β1 (DY240), Osteoprotegerin (OPG; DY805), receptor activator of nuclear factor kappa-B ligand (RANKL; DY626) and Connective Tissue Growth Factor (CTGF) (DY9190-05) were measured using Human DuoSet Enzyme linked immunosorbent assay (ELISA) kits (R&D Systems, Abingdon, United Kingdom) according to the manufacturer's instructions. Total RANKL was calculated by measuring free RANKL and in complex with OPG using an in house developed OPG/RANKL complex sandwich ELISA by using a human capture RANKL antibody (part of cat#DY626, R&D Systems) and a human detection OPG antibody (part of cat#DY805, R&D Systems) (Mogi and Kondo, 2010). Total OPG was calculated by measuring free OPG and bound OPG. To normalise ELISA data, cell numbers from ten fields of DAPI positive cells per donor on soft (±5 kPa) and stiff (±15 kPa) GelMA hydrogels were counted, and the total number of cells calculated for the overall GelMA hydrogel surface (1.9 cm^2) area.

2.11 Statistical analyses

Statistical analyses were performed using IBM SPSS Statistics for windows version 25 (IBM Corp., Armonk,

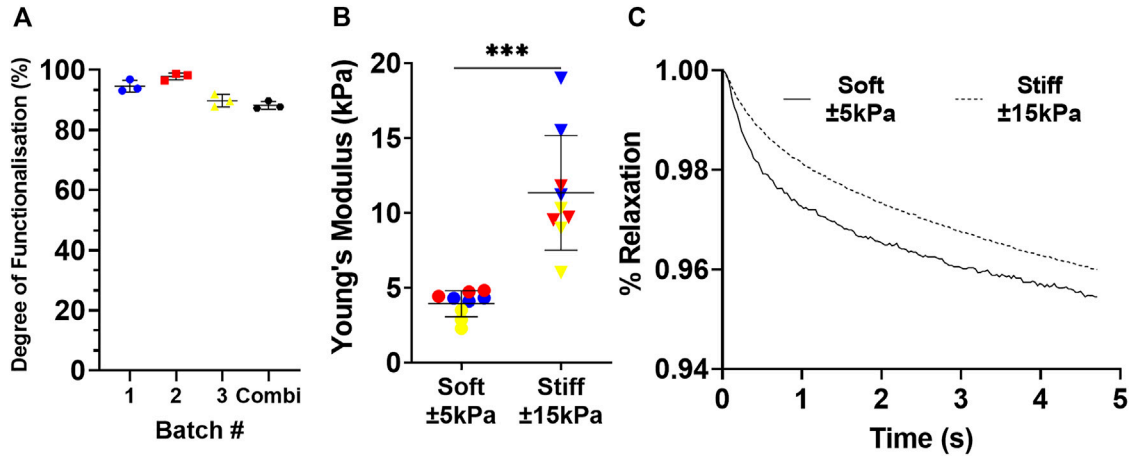

FIGURE 1
Mechanical properties of GelMA hydrogels. **(A)** Three different batches of GelMA were produced and the methacrylation efficiency was measured to demonstrate minimal variety before being combined into one large batch. Each dot represents a technical replicate of a batch. Data expressed as mean ± SD. Rheological properties were characterised by the Young's modulus of 3 different series **(B)**; blue, red and yellow) produced from three GelMA hydrogel solutions used in this study and the relaxation **(C)** over a period of 5 s. $n = 3$ with each dot representing a technical replicate of a unique sample. Data is expressed as mean ± SD in panel A–B, and mean in panel C ($n = 3$). Data were considered significant at $p < 0.05$.

N.Y., United States) and evaluated using Wilcoxon matched pair signed rank test for comparison between soft GelMA hydrogels and stiff GelMA hydrogels. Data were considered statistically significant at $p < 0.05$ unless stated otherwise. D'Agostino test was used to examine normality of the data and when necessary, log transformation applied. Correlations were assessed by calculating a Pearson correlation coefficient.

3 Results

3.1 Mechanical properties of GelMA hydrogels

Three different GelMA batches were produced and the methacrylation consistency was tested to determine if they could be combined into one large batch. The three different GelMA batches prepared for this study had a methacrylation efficiency of 94.58 ± 1.98%, 97.84 ± 1.14% and 89.77 ± 2.04% respectively (Figure 1A). The combined batch had a methacrylation efficiency of 88.22 ± 1.32%. Next, the Young's modulus was measured across a range of different percentage GelMA hydrogels of up to 10% GelMA (data not shown) to select the hydrogel composition with the stiffness that best mimicked healthy (±5 kPa) and fibrotic (±15 kPa) lung tissue. A hydrogel made of 5% wt/v GelMA resembled healthy tissue with Young's modulus of 3.94 kPa ±0.87 kPa whereas 8% wt% hydrogels most resembled stiff tissue with a Young's modulus of 11.34 kPa ±3.82 kPa (Figure 1B). To further characterise these hydrogels, relaxation was measured to see if the percentage of GelMA has an impact on relaxation. After initial compression of 20%, the dissipation of force was followed for a duration of 5 s (Figure 1C). The relaxation values were 4.54 ± 1.60% for 5% (soft) and 4.00 ± 0.32% for 8% (stiff) GelMA hydrogels.

3.2 Morphological differences of fibroblasts on soft and stiff GelMA hydrogels

To characterise responses of fibroblasts to their environment, fibroblasts were cultured on soft (±5 kPa) and stiff (±15 kPa) hydrogels and their morphology was observed after 1 and 7 days of culture. Fibroblasts seeded on both soft and stiff hydrogels exhibited a similar morphology after 24 h of culture (Figures 2A,B). After 7 days of culture, fibroblast morphology was also similar on both soft and stiff hydrogels (Figures 2A,B day 7). After observing a round morphology in some donors after 24 h a live/dead stain was performed to rule out apoptosis, which revealed live cells with no dead cells evident after 1 or 7 days of culture on either hydrogel (Figures 2C,D). Total fibroblast cell number after 7 days of culture was higher on stiffer hydrogels compared to soft hydrogels (Figure 2E) which is in concordance with literature in response to a stiff matrix. Morphology analysis using CellProfiler did not demonstrate major differences between fibroblast on day 1 or 7 and between soft and stiff hydrogels (Supplementary Figure S1).

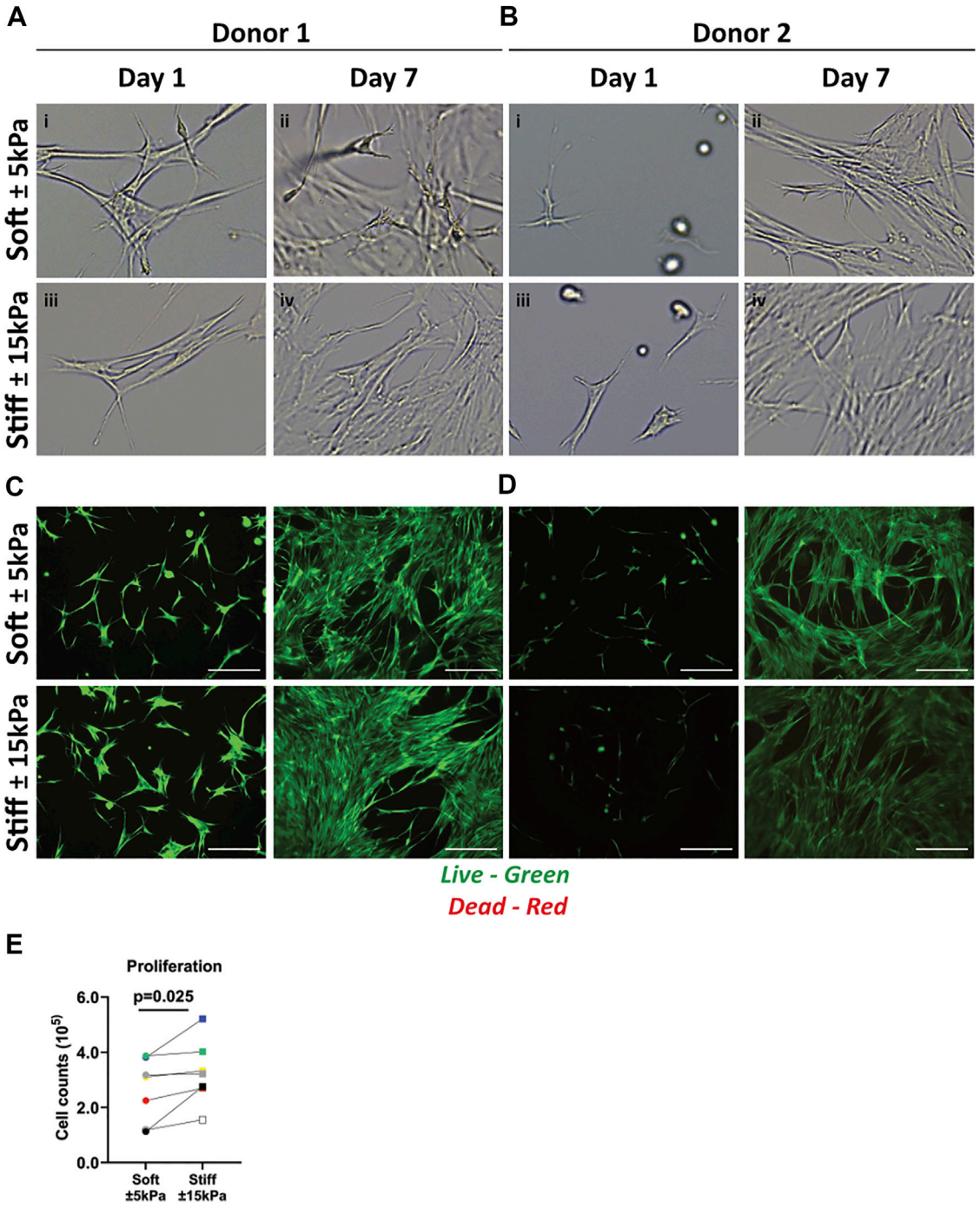

FIGURE 2
Primary human lung fibroblast morphology, live/dead staining and proliferation on soft (3.94 ± 0.87 kPa) and stiff (11.34 ± 3.82 kPa) GelMA hydrogels. **(A–B)** Representative brightfield microscopy images of cells 24 h post seeding and after 7 days of culture on top of soft and stiff hydrogels (digital magnification). Letters i-iv show areas of interest with different morphologies between donors. **(C,D)** Live (green) and dead (red) stain of two donors at day 1 and 7 of culture. **(E)** Total cell numbers on soft (3.94 ± 0.87 kPa) and stiff (11.34 ± 3.82 kPa) hydrogels after 7 days of cell culture. Images are representative of responses seen in 7 unique donors. (n = 7) Scale bar = 250 μm. Each donor has a different unique colour (blue, red, yellow, green, black, white, and grey).

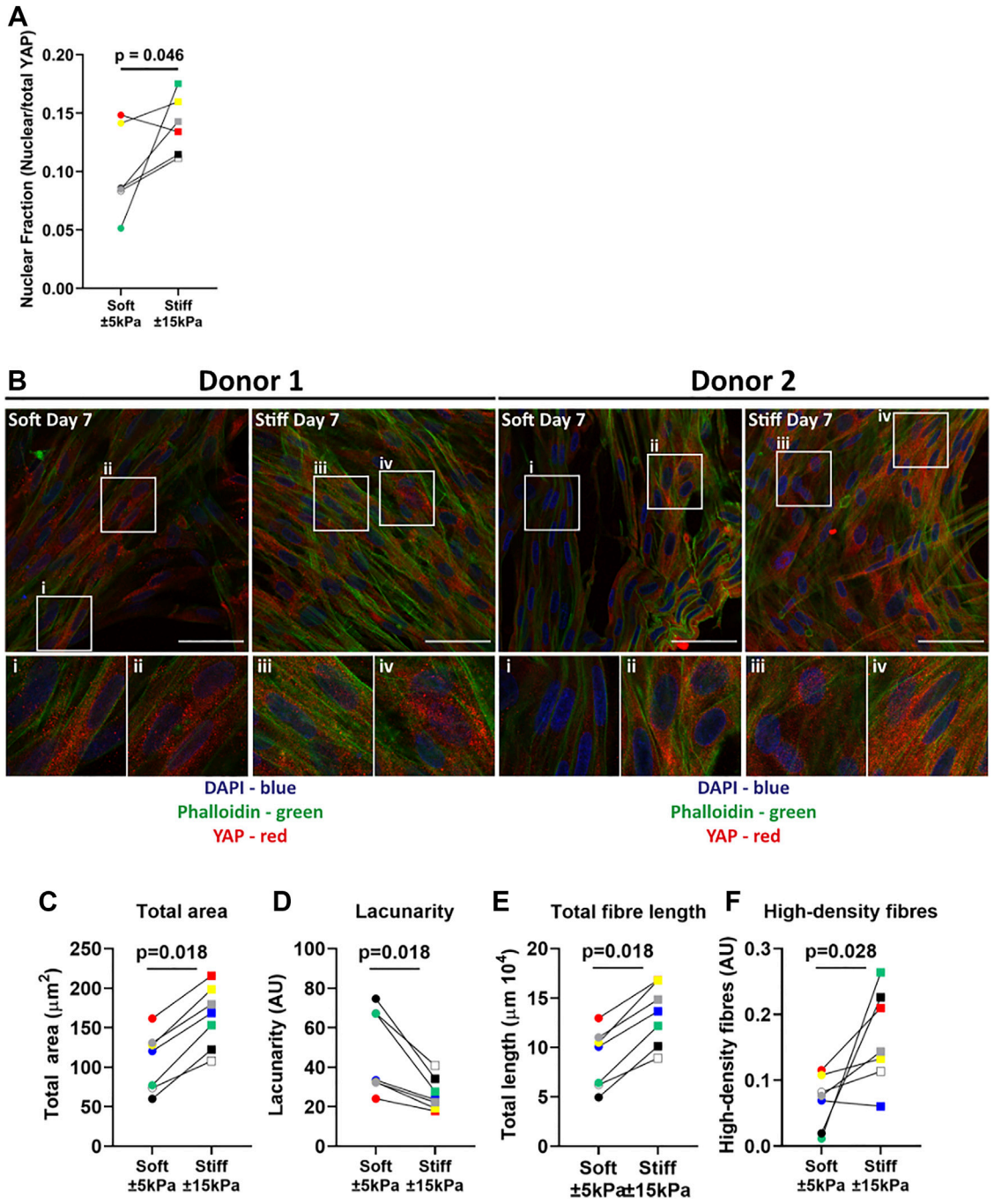

FIGURE 3
YAP translocation and F-actin stress fibre formation in primary human lung fibroblasts on soft (3.94 ± 0.87 kPa) and stiff (11.34 ± 3.82 kPa) hydrogels. Hydrogels after 7 days of culture were fixed and fibroblasts were stained for YAP and F-actin. **(A)** Quantification of YAP nuclear fraction **(B)** representative fluorescent images of DAPI (Blue), YAP (Red) and F-actin (green). i-iv) White boxes show the region of interest that is magnified. TWOMBLI analyses of phalloidin stained fibroblasts showing total area **(C)**, lacunarity **(D)**, fibre length **(E)** and high-density fibre networks **(F)** (calculated using the high-density matrix algorithm). Images are representative of responses seen in 7 unique donors. (n = 6–7) Scale bar = 50 μm. Each donor has a different unique colour (blue, red, yellow, green, black, white, and grey).

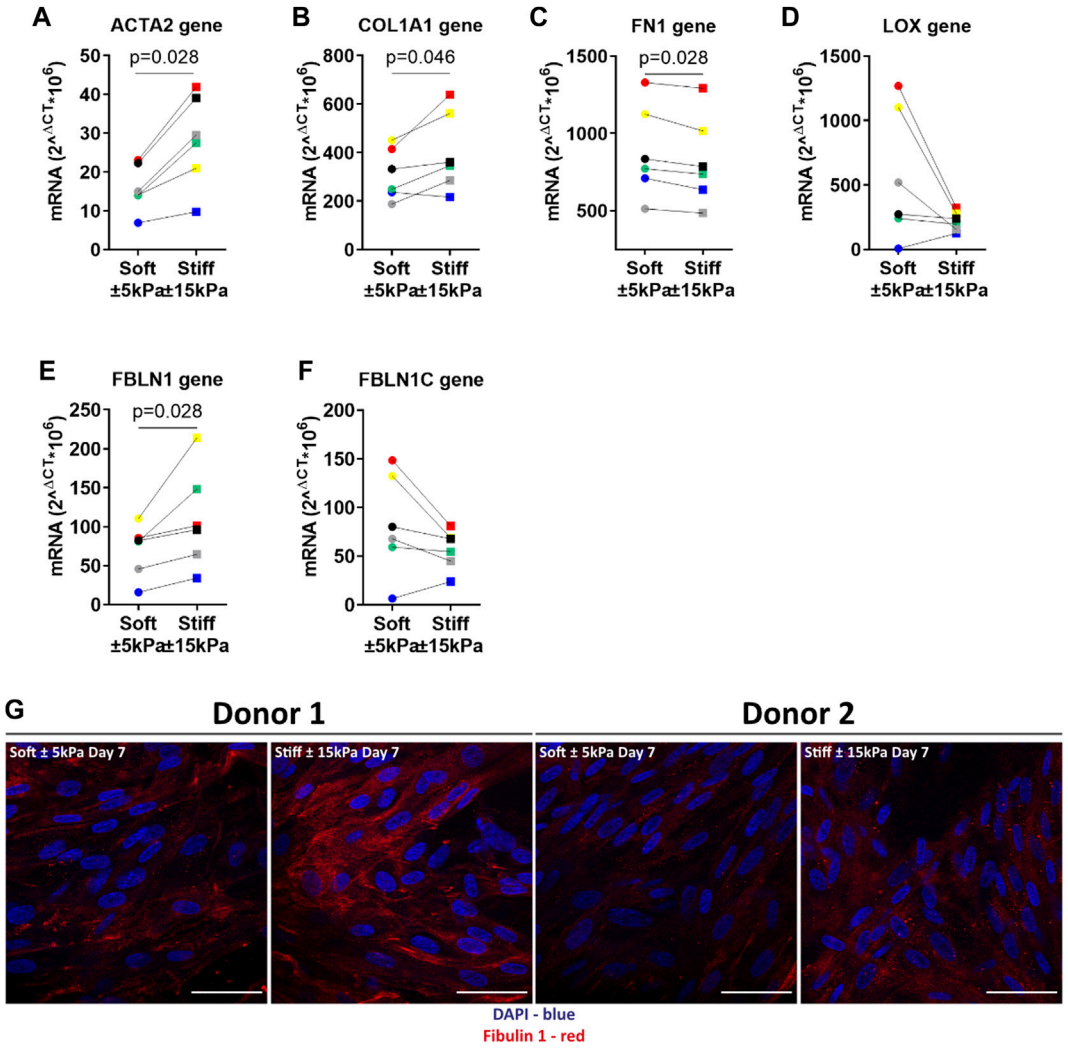

FIGURE 4
Primary human lung fibroblast markers of cellular senescence in response to surface stiffness. **(A–C)** Gene expression of the cell-cycle inhibitors *p21*$^{Waf1/Cip1}$ *and p16*^{Ink4a}, *p53* and known SASP factors *IL-6* and *CXCL8* after 7 days of culture, data were normalised against 18S and expressed as $2^{-\Delta CT}$ x 10^6. **(D-G)** Levels of SASP cytokine production in supernatant, data were normalised to cell numbers and are expressed as pg/mL per 10^5 cells. Differences between soft (3.94 ± 0.87 kPa) and stiff (11.34 ± 3.82 kPa) hydrogels were analysed by a Wilcoxon matched pairs signed rank test (n = 6) and $p < 0.05$ was considered significant. Each donor has a different unique colour (blue, red, yellow, green, black, and grey).

3.3 Increased total yes-associated protein-1 content and organised F-actin formation in fibroblasts on stiffer matrices

Next, the mechanosensory response of fibroblasts to their environment was examined using a dual stain for Yes-associated protein 1 (YAP) nuclear translocation and F-actin fibre formation. The YAP nuclear fraction was higher on stiff hydrogels compared to soft hydrogels (Figure 3A). Figure 3B shows the nuclear translocation of YAP on soft and stiff hydrogels on day 7. F-actin cytoskeleton arrangement in fibroblasts on soft hydrogels was composed of both diffuse and organised F-actin fibres, while fibroblasts on stiffer hydrogels display bundled organised F-actin fibres (Figure 3B), indicative of their responsiveness to the substrate stiffness. To quantify the differences in ECM patterns between soft and stiff hydrogels we measured several parameters using the TWOMBLI plugin. Figure 3C demonstrates that there is a clear increase in total area of F-actin fibres in fibroblasts cultured on stiff hydrogels. This is supported by the reduction in space between the fibres (Figure 3D) as well as the increase in F-actin fibre length (Figure 3E). Lasty, we measured a strong increase in the high-density fibre network, which confirms areas with increased tight f-actin bundles formed in response to stiffness (Figure 3F).

10.3389/fphar.2022.989169

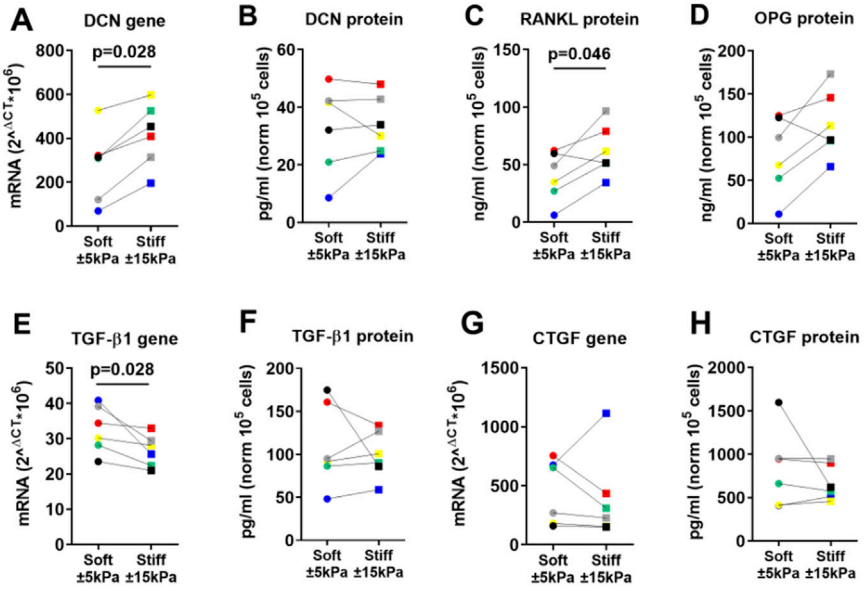

I

		IL-6	CXCL8	TGF-β1	CTGF	OPG	RANKL	DCN
OPG	Pearson r	0.84600	0.85900	0.81500	0.62800		0.98600	0.48008
	p value	5.26E-04	3.40E-04	1.25E-03	2.88E-02		4.75E-09	1.14E-01
RANKL	Pearson r	0.82900	0.84500	0.78400	0.57061	0.98600		0.40576
	p value	8.64E-04	5.45E-04	2.55E-03	5.27E-02	4.75E-09		1.91E-01

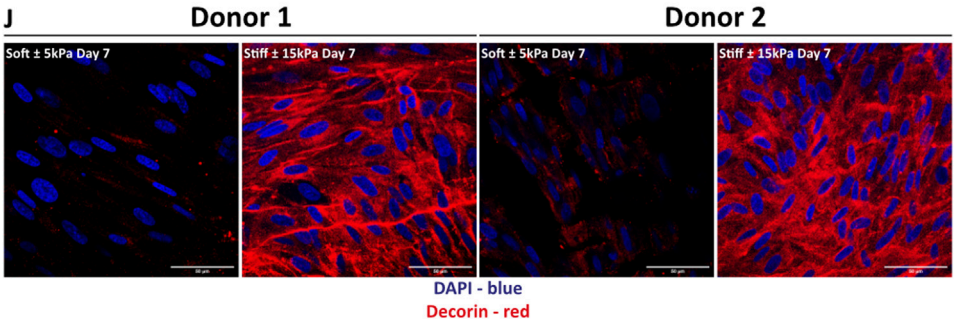

FIGURE 5
Stiffness induced a secretory phenotype in Primary human lung fibroblasts cultured on stiff matrices. **(A,B)** DCN gene expression and secreted protein were measured after 7 days of culture on soft (3.94 ± 0.87 kPa) and stiff (11.34 ± 3.82 kPa) hydrogels. **(C–H)** Levels of secreted factors RANKL, OPG, CTGF and TGF-β1 including TGF-β1 and CTGF gene expression after 7 days of culture on soft and stiff hydrogels. I) Correlation was calculated between OPG, RANKL and all other secreted factors. Panel J shows a fluorescent staining for DCN, DAPI was used for identification of cell nuclei. Illustrated photographs are representative images of in total 7 unique donors. Gene expression data were normalised against 18S and expressed as $2^{-\Delta CT}$ x 10^6. Secreted matrix proteins and cytokines were normalised to cell counts and expressed as pg/ml or ng/ml 10^5 cells. Differences between soft and stiff hydrogels were analysed by a Wilcoxon matched pairs signed rank test. Correlation was calculated using Pearson correlation coefficient. (n = 6) Scale bar = 50 μm. Each donor has a different unique colour (blue, red, yellow, green, black, and grey).

3.4 Higher matrix stiffness does not contribute to cellular senescence in fibroblasts

After confirming that fibroblasts respond to their environment, we explored our hypothesis that increased stiffness may contribute to the senescent state. Therefore, several biomarkers for senescence were analysed in fibroblasts grown on soft and stiff hydrogels mimicking healthy and diseased tissue stiffnesses. Gene expression analysis of early-stage marker *p21*$^{Waf1/Cip1}$ did not demonstrate a difference while late-stage senescence marker *p16*^{Ink4a} demonstrated a trend ($p = 0.075$) towards an increase between soft and stiff hydrogels (Figures 4B,C). Interestingly, *p53* demonstrated a trend towards a decrease in fibroblasts on stiff hydrogels (Figure 4C). To further characterise cellular senescence, both gene expression and secretion of the well characterised SASP factors IL-6 and CXCL8 were measured (Figures

4D–G). Gene expression of *IL-6* was significantly higher on stiffer hydrogels (Figure 4D). However, the secretion of IL-6 did not change between soft and stiff hydrogels. Both CXCL8 gene and protein expression did not exemplify a difference between soft and stiff hydrogels after 7 days of culture (Figures 4F,G).

3.5 Higher matrix stiffness induces a secretory phenotype in primary fibroblasts

Our data indicated that there was no greater activation of the cell-cycle inhibitors $p16^{Ink4a}$ and $p21^{Waf1/Cip1}$ on stiffer hydrogels compared to softer hydrogels, but rather an increase in proliferation. To further characterise the activation of a secretory phenotype we measured several factors that have been reported to be part of the senescent phenotype and/or to be part of a fibrotic response (Verrecchia and Mauviel, 2007; Coppe et al., 2010; Zhang et al., 2018; Faget et al., 2019). Gene expression and secreted protein levels of the proteoglycan DCN were higher on stiff compared to soft hydrogels (Figure 5A). Next, RANKL was measured as it was recently shown to be secreted by senescent fibroblasts in COPD (Woldhuis et al., 2020a). RANKL secretion was significantly higher at day 7 on stiffer hydrogels while its decoy receptor OPG showed a trend towards an increase at day 7 on stiffer hydrogels (Figures 5C,D). Additionally, TGF-β1 gene expression and protein secretion were measured. TGF-β1 gene expression demonstrated a significant decrease on stiff hydrogels compared to soft hydrogels (Figures 5E,F) while there was no change in protein secretion (Figure 5G). Finally, CTGF gene expression and secretion were measured, which demonstrated no difference for secretion between soft and stiffer hydrogels at day 7 while gene expression demonstrated a trend towards a decrease (Figures 5G,H). To explore if the OPG-RANKL axis serves as a mechanism that potentially could have an effect on both fibrosis and senescence, we explored the correlation between OPG-RANKL and other secreted factors (Figure 5I). Correlations for both OPG and RANKL were observed with IL-6, CXCL8 and TGF-β1. CTGF was correlated with OPG but not RANKL, and no correlations were observed with DCN. Additionally, we stained the cells on the surfaces of the hydrogels for DCN protein levels. Figure 5J shows the DCN stain on both soft and stiffer hydrogels after 7 days in culture. DCN displayed a strong visual increase on the stiffer hydrogels in comparison to the soft hydrogels.

3.6 Matrix stiffness activates a profibrotic response in primary fibroblasts

To further characterise the fibrotic response of fibroblasts on stiffer hydrogels we measured several fibrosis-associated genes. Previous studies have reported that higher expression of these genes is associated with persistent fibroblast activation and higher ECM deposition in fibrosis. Lung fibroblasts on stiffer hydrogels exhibited higher α-SMA and COL1α1 expression after 7 days of culture compared to soft hydrogels (Figures 6A,B). The expression of FN1 was significantly lower after 7 days on stiffer hydrogels (Figure 6C). Interestingly, LOX gene expression was lower in cells grown on stiff hydrogels compared to soft hydrogels (Figure 6D). Fibulin-1 gene expression was higher after 7 days on stiffer hydrogels (Figure 6E). However, FBLN1C gene expression was not different between cells grown on soft or stiffer hydrogels (Figure 6F). The final characterisation was an immunofluorescent staining for deposited FBLN1 on both soft and stiffer hydrogels at day 7. We visualised a higher deposition of FBLN1 on stiffer hydrogels in comparison to soft hydrogels (Figure 6G).

4 Discussion

During fibrotic disease, the ECM undergoes tremendous change that influence the composition and stiffness of the tissue. These changes have a substantial effect on cell function, and it has been reported that fibrotic ECM is able to create a profibrotic positive feedback loop (Parker et al., 2014). In the present study we created hydrogels reflecting the approximate median pathological stiffness measured in fibrotic diseases and examined the impact on cellular responses of lung fibroblasts focusing on markers of senescence, including the SASP and fibrosis. Pathological stiffness did not affect $p16^{Ink4a}$,$p21^{Waf1/Cip1}$ or *p53*, the main markers of senescence, instead it resulted in higher expression of genes/proteins associated with the SASP and fibrosis such as *IL-6*, *ACTA2, COL1A1*, *FBLN1* and *DCN* compared to soft matrix. However, some markers including IL-6, OPG and RANKL are identified to be both expressed/secreted during cellular senescence and different stages of fibrosis. Collectively, the data presented in this study suggest that exposure of fibroblasts to a surface within the range of pathological stiffness modulates gene expression and secreted factors that are both involved in cellular senescence and the fibrotic response in fibroblasts.

Methacrylated-gelatine gels are well characterised hydrogels that support growth of a large variety of cells, that are biodegradable, that allow cell adhesions through Arg-Gly-Asp (RGD) sequences and allow for precise tuning of mechanical properties. Precise tuning of the degree of functionalisation, gelatine concentration and number of crosslinks results in high reproducibility and controllability of biophysiochemical properties (Schuurman et al., 2013; Zhu et al., 2019; Tabatabaei et al., 2020). These characteristics made these hydrogels ideal for our study. In this study we generated two hydrogels with a different Young's modulus while the initial stress relaxation behaviour did not significantly change. This was not unexpected as both hydrogels were almost equal in their constituent biomaterials, reflecting the difference in

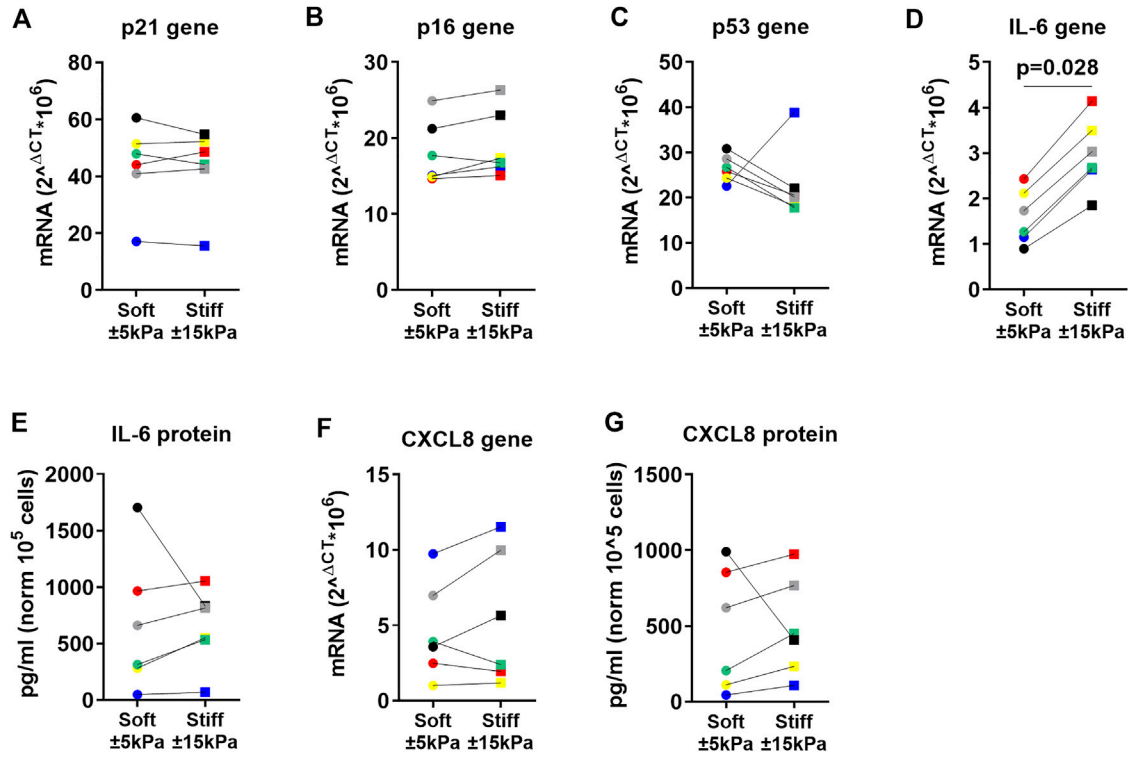

FIGURE 6
Primary human lung fibroblasts exhibit an activated and profibrotic phenotype on stiff (11.34 ± 3.82 kPa) compared to soft (3.94 ± 0.87 kPa) hydrogels. To characterise the fibrotic response of fibroblasts on hydrogels, gene expression levels for fibroblast activation α-SMA and matrix proteins COL1α1, FN1, LOX, FBLN1 and FBLN1C were measured at day 7 **(A–F)**. Finally, deposited FBLN1 (Red) was stained using fluorescent labelled antibodies and DAPI for identification of cell nuclei in panel **(G)**. Illustrated photographs are representative images of in total 7 donors. Differences between soft and stiff hydrogels were analysed by a Wilcoxon matched pairs signed rank test (n = 6). Scale = 50 μm. Each donor has a different unique colour (blue, red, yellow, green, black, and grey).

percentage of GelMA used. This observation authenticates that the responses of the fibroblasts measured herein could be contributed to the differences in Young's modulus only. However, more focus is directed towards the effect of stress relaxation and how it may influence cell behaviour (Chaudhuri et al., 2015; Chaudhuri et al., 2020). Tests on tissues such as liver, skin, muscle, and breast reveal that these organs dissipate stress ranging from milliseconds to hundreds of seconds (McKinnon et al., 2014; Chaudhuri et al., 2016). Changes in viscoelastic properties have been associated with disease progression including cancer. Substrate stiffness has a robust effect on cell function and regulates cell viability, proliferation, migration, differentiation, and cell-matrix adhesion (Huang et al., 2012). Higher proliferation, contractility and activation of fibroblasts are all reported as responses to a stiffer environment (Balestrini et al., 2012; Asano et al., 2017; Sun et al., 2018). In this regard, the proliferation and high viability of fibroblasts grown on both soft and stiffer hydrogels observed in this study were comparable to observations from previous investigations (Solon et al., 2007; Asano et al., 2017; Ruiz-Zapata et al., 2020). Furthermore, the morphology of fibroblasts on soft gels was comparable to fibroblasts on stiffer gels. This is in contrast to some literature where it is shown that there is little spread of cells on soft stiffness (Solon et al., 2007). However, the stiffness representing a soft matrix is often much lower than used in this study and is more in the range of 0.5 kPa In addition, culture times were also different which potentially contributes to the morphology as fibroblasts produce matrix of their own which facilitates attachment. Furthermore, differences in gel composition may also contribute to this effect, for example polyacrylamide has no RGD sequences as are present in GelMA due to its biological origin, and this may impact on the ability of the fibroblasts to attach and spread on the gel surface.

In response to mechanical cues such as stiffness, fibroblasts organise their actin fibres and translocate YAP into the nucleus leading to cellular activation and transcription of genes in many cell types (Dupont et al.,

2011; Raghunathan et al., 2013; Liu et al., 2015). The data in this study showed that total YAP content in fibroblasts is higher on stiffer compared to soft hydrogels and that organised bundled F-actin fibres are formed, which is indicative of the cells responding to the mechanical environment. However, there was an apparent lack of nuclear staining for YAP at day 7 in the fibroblasts on either hydrogel, particularly in regions of higher cell density. This may be explained by the fact that YAP becomes less mechanosensitive and remains in the cytoplasm as a response to cell-cell interactions (Das et al., 2016; Totaro et al., 2017). Furthermore, while increased nuclear translocation is well documented in response to a stiffer environment, the increase in total YAP is not yet clarified. In fact, stimulation with TGF-β1 demonstrated a reduction in YAP mRNA expression in the first 24 h while protein levels did not change (Piersma et al., 2015b). Moreover, the formation of organised bundled actin may also contribute to this effect by altering the shape of the nuclear envelope which potentially changes the environment for transcription and thus impacting on fibroblast function (Zhao et al., 2007). Little is known about the interplay between an altered ECM and cellular senescence, therefore after confirming that, in our model, fibroblast respond to their substrate, we investigated what the contribution was of increased stiffness on cellular senescence and the SASP. The results from the present study provided evidence that there was an increase of proliferation and modulation of some markers of senescence in response to pathological stiffness at day 7. Higher cell proliferation and migration, as reflected in our study, has been widely documented as a result of increased matrix stiffness and is part of an important response to injury in wound repair (Reinke and Sorg, 2012; Wickert et al., 2016). Interestingly, we also observed an increase in *IL-6* gene expression and a trend towards an increase in CXCL8 protein secretion in the stiffer environment. Both pro-inflammatory cytokines are involved in wound repair and are identified as part of the SASP, which plays an important role in fibrosis (Coppe et al., 2010; Schafer et al., 2017). Furthermore, there is evidence suggesting that the SASP can be activated independently of cell-cycle inhibitors $p16^{Ink4a}$ and $p21^{Waf1/Cip1}$ in cellular senescence (Coppe et al., 2011; Wang et al., 2017). Activation of the SASP might be an early indicator of senescence and precedes the irreversible cell-cycle arrest of premature cellular senescence.

Activation of a secretory phenotype is beneficial for tissue repair, but it can also be detrimental and contribute to disease progression in fibrosis (Pratsinis et al., 2019). Our results showed activation of a secretory phenotype in response to increased surface stiffness, including a strong correlation of RANKL and OPG with other secreted factors, but not DCN. All of these factors have been recognised to be part of the SASP and/or to be part of the fibrotic response. DCN is recognised for its role in many different biological processes and recently DCN has been found negatively correlated with $p16^{Ink4a}$ in senescence in COPD (Woldhuis et al., 2020b). Our results suggest, in the context of fibrosis, that DCN deposition is in response to stiffer hydrogels, further supporting the important role DCN plays in fibrosis (Westergren-Thorsson et al., 2004; Zhang et al., 2018). CTGF is an important mediator in tissue remodelling and has been associated with senescence, fibrosis and cancer (Riser et al., 2015; Jun and Lau, 2017). CTGF can be regulated *via* its main inducer TGF-β1 or can be negatively regulated by DCN and OPG (Vial et al., 2011; Aoyama et al., 2015). Given the fact that, in our study, TGF-β1 secretion was unaltered and an increase in DCN secretion was observed, it was not surprising that no change in CTGF secretion was found in response to increasing stiffness. CTGF has also been reported to be downstream of YAP, and we reported there was more YAP retention in the cytoplasm potentially contributing to less upregulation in response to the stiffer environment (Davis and Foster, 2018; Shome et al., 2020). In addition, there was downregulation of CTGF gene expression in response to stiffer hydrogels confirming the findings that protein secretion was unaltered. The RANKL-OPG system is essential for bone metabolism, where OPG acts as a decoy receptor for RANKL, regulating development and activity of osteoclasts. OPG is currently used as a biomarker for liver fibrosis (Coppe et al., 2010; Adhyatmika et al., 2020), while RANKL was recently identified to be part of the SASP in senescent COPD fibroblasts (Woldhuis et al., 2020a). In IPF the exact role of OPG is not fully understood but evidence suggests it may play a role in active fibrosis and associates with disease progression (Wang et al., 2019; Habibie et al., 2020). Our correlation analysis between RANKL, OPG and other secreted factors demonstrated a strong correlation. These factors, such as TGF-β1 and CTGF, are part of both the SASP and fibrotic response. It might be possible that RANKL as a SASP and OPG as a fibrotic-associated marker create a regulatory pathway between the senescent and fibrotic response in stiff lung tissues. Moreover, CTGF has been identified to bind to OPG and might be a potential fourth factor in the RANK-RANKL-OPG system, potentially contributing to the regulatory mechanism as well (Lipson et al., 2012; Aoyama et al., 2015; Jun and Lau, 2017; Kim et al., 2020). This mechanism might also contribute to the fact that we did not measure any difference in protein secretion, despite lower mRNA levels. Taken together these data suggest that the RANKL-OPG-CTGF system may contribute to secreted factor regulation, increased ECM deposition and potentially contribute to the progression/perpetuation of fibrosis in response to a stiffer tissue environment as central regulator.

Fibroblasts can be activated in response to increased stiffness leading to higher expression of α-SMA and matrix proteins, which is part of a normal wound repair response after injury. Our

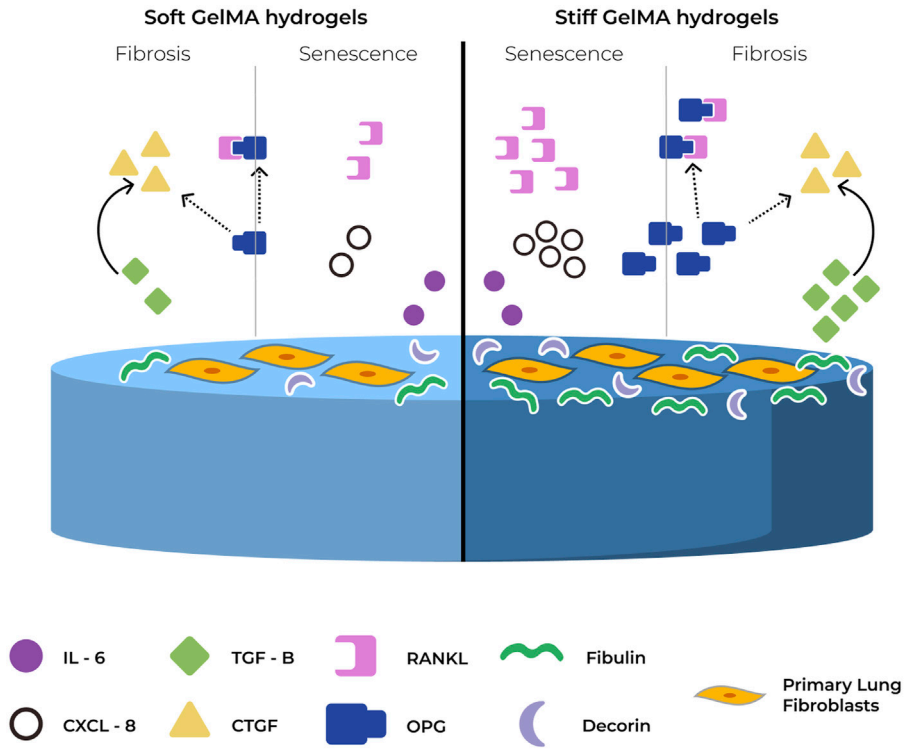

FIGURE 7
Summary of proposed mechanism for OPG in senescence and fibrosis. In response to stiffness, Primary human lung fibroblasts show increased proliferation, higher deposition of ECM proteins and higher secretion of SASP and fibrosis related cytokines. OPG is proposed to act as a regulatory mechanism between senescence and fibrosis by binding to RANKL and CTGF, and potentially inhibiting their function.

results indicate that in response to stiffer hydrogels fibroblasts show upregulation of several fibrosis associated genes including *ACTA2* and *COL1A1*. Increase in *FBLN1* expression and deposition on stiffer hydrogels was expected and is in line with what has been reported in literature (Paapstel et al., 2016; YasminMaskari et al., 2018). However, the lack of response of *FBLN1C* gene expression was unexpected as *FBLN1C* has been reported to be implicated in fibrosis and lung injury (Ge et al., 2015; Liu et al., 2019). However, it has been reported that TGF-β1, which is unaltered in our study, downregulates *FBLN1* gene expression and promotes FBLN1 deposition in airway smooth muscle cells (Chen et al., 2013). This could indicate that FBLN1/C regulation might be cell-type and disease specific. Interestingly, FN1 which is associated with FBLN1 was decreased on stiffer hydrogels after 7 days. This was in contrast with literature where FN1 was shown to be an important mediator of early wound repair, collagen fibril formation and fibrosis (Valiente-Alandi et al., 2018). Additionally, Zhou and others demonstrated that FN1 expression increased when primary lung fibroblasts were cultured for up to 48 h on stiff matrixes (Zhou et al., 2020). However, it is possible that FN1 peaked early in the time-course of our experiment, especially given its role in the initial phase of wound repair and had subsequently decreased at the time we measured it. Finally, *LOX* gene expression demonstrated a fine regulation by stiffer hydrogels regardless of gene expression on soft hydrogels. LOX is implicated in fibrosis and its role is disease specific (Huang et al., 2019; Nguyen et al., 2021). For example, in renal and liver fibrosis increased LOX expression leads to ECM production and progression of fibrosis (Ikenaga et al., 2017). In IPF, LOX gene expression did not change between healthy and IPF. However, on protein level it was reported that LOX deposition was decreased in IPF tissue (Tjin et al., 2017). Therefore, it would be appropriate to determine enzyme activity as gene and protein expression do not always correlate.

The experimental strategy used in this study was designed to measure the impact of stiffness on the senescent phenotype in fibroblasts after 7 days in culture. While there was modulation of some markers of cellular senescence, other studies investigating senescence induce this by stimulating the cells with paraquat or hydrogen peroxide (Waters et al., 2019; Woldhuis et al., 2020b). It is possible that the early senescence marker $p21^{Waf1/Cip1}$ reached its highest expression before we assessed the expression at day 7, while still being too early to detect high levels of $p16^{Ink4a}$. In several of our datasets there appear to be data points driving the lack of statistical

difference, however, these are not attributed to a single donor but rather represent different donors in each dataset. This variability can be attributed to the biological heterogeneity of the primary lung fibroblasts used in this study. Cell numbers at the start of the study were optimised for measuring senescence readouts. This made the assessment of YAP translocation challenging as the density of fibroblasts on day 7 were higher than optimal for this readout. In addition, YAP translocation is a swift process as cytoplasmic/nuclear levels can be stable within 1 day after changing the stiffness (Zhang et al., 2021). This could have implications for measuring YAP translocation as the regulatory effect may have been partially diminished demonstrating a weaker effect.

In conclusion, we have established that the culture of human lung fibroblasts on matrices that mimic pathological stiffness within the range of fibrotic tissues for up to 7 days leads to activation of genes and secretion of matrix proteins and cytokines that are part of the fibrotic response, with overlap of SASP factors (Figure 7). Our data suggest that there may be an overlap between cellular senescence/SASP and the fibrotic response, indicating that the fibroblasts may acquire a pre-senescent and/or activated phenotype. The modulation of cell function in response to pathological stiffness may ultimately lead to the creation of a negative feedback loop in which pre-senescent and/or activated fibroblasts reinforce each other causing a perpetuating cycle driving aberrant ECM accumulation and progression of a fibrotic response.

Data availability statement

The raw data supporting the conclusions of this article will be made available by the authors, without undue reservation.

Ethics statement

Ethical review and approval was not required for the study on human participants in accordance with the local legislation and institutional requirements. Written informed consent for participation was not required for this study in accordance with the national legislation and the institutional requirements.

Author contributions

KB, MN, MS, DK, CB, SP, and JB conceived and designed research; KB and MN performed experiments; KB, MN, HH, and TB analysed data; KB, MN, HH, MS, BM, DK, CB, SP, and JB interpreted results; KB and MN prepared figures; KB, MN, HH, and TB writing–original draft; KB, MN, HH, TB, MS, BM, DK, CB, SP, and JB Writing–review and editing. All authors have read and agreed to the final version of the manuscript. All authors have access to the raw data and BM, CB, SP, and JB can verify the raw data in this study.

Funding

KB was supported by De Cock—Hadders Foundation research grant 2020-48, and the UMCG Abel Tasman Scholarship. JB was supported by a Rosalind Franklin Fellowship (co-funded by the University of Groningen and European Union), and the Nederlandse Organisatie voor Wetenschappelijk Onderzoek (NWO) Aspasia-premie subsidienummer 015.013.010.

Acknowledgments

The authors thank M.R. Jonker, L. Apperloo and G.J. Teitsma for their technical assistance in this study.

Publisher's note

Supplementary material

The Supplementary Material for this article can be found online at: https://www.frontiersin.org/articles/10.3389/fphar.2022.989169/full#supplementary-material.

References

Adhyatmika, A., Beljaars, L., Putri, K. S. S., Habibie, H., Boorsma, C. E., Reker-Smit, C., et al. (2020). Osteoprotegerin is more than a possible serum marker in liver fibrosis: A study into its function in human and murine liver. *Pharmaceutics* 12 (5), 471. doi:10.3390/pharmaceutics12050471

Aoyama, E., Kubota, S., Khattab, H. M., Nishida, T., and Takigawa, M. (2015). CCN2 enhances RANKL-induced osteoclast differentiation via direct binding to RANK and OPG. *Bone* 73, 242–248. doi:10.1016/j.bone.2014.12.058

Asano, S., Ito, S., Takahashi, K., Furuya, K., Kondo, M., Sokabe, M., et al. (2017). Matrix stiffness regulates migration of human lung fibroblasts. *Physiol. Rep.* 5 (9), e13281. doi:10.14814/phy2.13281

Balestrini, J. L., Chaudhry, S., Sarrazy, V., Koehler, A., and Hinz, B. (2012). The mechanical memory of lung myofibroblasts. *Integr. Biol.* 4 (4), 410–421. doi:10.1039/c2ib00149g

Blokland, K. E. C., Pouwels, S. D., Schuliga, M., Knight, D. A., and Burgess, J. K. (2020). Regulation of cellular senescence by extracellular matrix during chronic fibrotic diseases. *Clin. Sci.* 134 (20), 2681–2706. doi:10.1042/CS20190893

Blokland, K. E. C., Waters, D. W., Schuliga, M., Read, J., Pouwels, S. D., Grainge, C. L., et al. (2020). Senescence of IPF lung fibroblasts disrupt alveolar epithelial cell proliferation and promote migration in wound healing. *Pharmaceutics* 12 (4), E389. doi:10.3390/pharmaceutics12040389

Bonnans, C., Chou, J., and Werb, Z. (2014). Remodelling the extracellular matrix in development and disease. *Nat. Rev. Mol. Cell Biol.* 15 (12), 786–801. doi:10.1038/nrm3904

Booth, A. J., Hadley, R., Cornett, A. M., Dreffs, A. A., Matthes, S. A., Tsui, J. L., et al. (2012). Acellular normal and fibrotic human lung matrices as a culture system for *in vitro* investigation. *Am. J. Respir. Crit. Care Med.* 186 (9), 866–876. doi:10.1164/rccm.201204-0754OC

Chaudhuri, O., Cooper-White, J., Janmey, P. A., Mooney, D. J., and Shenoy, V. B. (2020). Effects of extracellular matrix viscoelasticity on cellular behaviour. *Nature* 584 (7822), 535–546. doi:10.1038/s41586-020-2612-2

Chaudhuri, O., Gu, L., Darnell, M., Klumpers, D., Bencherif, S. A., Weaver, J. C., et al. (2015). Substrate stress relaxation regulates cell spreading. *Nat. Commun.* 6 (1), 6364. doi:10.1038/ncomms7365

Chaudhuri, O., Gu, L., Klumpers, D., Darnell, M., Bencherif, S. A., Weaver, J. C., et al. (2016). Hydrogels with tunable stress relaxation regulate stem cell fate and activity. *Nat. Mat.* 15 (3), 326–334. doi:10.1038/nmat4489

Chen, L., Ge, Q., Black, J. L., Deng, L., Burgess, J. K., and Oliver, B. G. (2013). Differential regulation of extracellular matrix and soluble fibulin-1 levels by TGF-β1 in airway smooth muscle cells. *PLoS One* 8 (6), e65544. doi:10.1371/journal.pone.0065544

Coppe, J. P., Desprez, P. Y., Krtolica, A., and Campisi, J. (2010). The senescence-associated secretory phenotype: The dark side of tumor suppression. *Annu. Rev. Pathol.* 5 (1), 99–118. doi:10.1146/annurev-pathol-121808-102144

Coppe, J. P., Rodier, F., Patil, C. K., Freund, A., Desprez, P. Y., and Campisi, J. (2011). Tumor suppressor and aging biomarker p16(INK4a) induces cellular senescence without the associated inflammatory secretory phenotype. *J. Biol. Chem.* 286 (42), 36396–36403. doi:10.1074/jbc.M111.257071

Das, A., Fischer, R. S., Pan, D., and Waterman, C. M. (2016). YAP nuclear localization in the absence of cell-cell contact is mediated by a filamentous actin-dependent, myosin II- and phospho-YAP-independent pathway during extracellular matrix mechanosensing. *J. Biol. Chem.* 291 (12), 6096–6110. doi:10.1074/jbc.M115.708313

Davis, J. T., and Foster, W. J. (2018). Substrate stiffness influences the time dependence of CTGF protein expression in muller cells. *Int. Physiol. J.* 1 (1), 1. doi:10.14302/issn.2578-8590.ipj-17-1910

de Hilster, R. H. J., Sharma, P. K., Jonker, M. R., White, E. S., Gercama, E. A., Roobeek, M., et al. (2020). Human lung extracellular matrix hydrogels resemble the stiffness and viscoelasticity of native lung tissue. *Am. J. Physiol. Lung Cell. Mol. Physiol.* 318 (4), L698–L704. doi:10.1152/ajplung.00451.2019

Dupont, S., Morsut, L., Aragona, M., Enzo, E., Giulitti, S., Cordenonsi, M., et al. (2011). Role of YAP/TAZ in mechanotransduction. *Nature* 474 (7350), 179–183. doi:10.1038/nature10137

Faget, D. V., Ren, Q., and Stewart, S. A. (2019). Unmasking senescence: Context-dependent effects of SASP in cancer. *Nat. Rev. Cancer* 19 (8), 439–453. doi:10.1038/s41568-019-0156-2

Foucher, J., ChantEloup, E., Vergniol, J., Castera, L., Le Bail, B., Adhoute, X., et al. (2006). Diagnosis of cirrhosis by transient elastography (FibroScan): A prospective study. *Gut* 55 (3), 403–408. doi:10.1136/gut.2005.069153

Ge, Q., Chen, L., Jaffar, J., Argraves, W. S., Twal, W. O., Hansbro, P., et al. (2015). Fibulin1C peptide induces cell attachment and extracellular matrix deposition in lung fibroblasts. *Sci. Rep.* 5 (1), 9496. doi:10.1038/srep09496

Habibie, H., Putri, K. S. S., Boorsma, C. E., Brass, D. M., Heukels, P., Wijsenbeek, M., et al. (2020). Osteoprotegerin is elevated in pulmonary fibrosis and associates with IPF progression. *bioRxiv*. doi:10.1101/2020.12.02.408062

Hansen, N. U., Genovese, F., Leeming, D. J., and Karsdal, M. A. (2015). The importance of extracellular matrix for cell function and *in vivo* likeness. *Exp. Mol. Pathol.* 98 (2), 286–294. doi:10.1016/j.yexmp.2015.01.006

Hinz, B. (2012). Mechanical aspects of lung fibrosis: A spotlight on the myofibroblast. *Proc. Am. Thorac. Soc.* 9 (3), 137–147. doi:10.1513/pats.201202-017AW

Huang, M., Liu, Z., Baugh, L., Defuria, J., Maione, A., Smith, A., et al. (2019). Lysyl oxidase enzymes mediate TGF-β1-induced fibrotic phenotypes in human skin-like tissues. *Lab. Invest.* 99 (4), 514–527. doi:10.1038/s41374-018-0159-8

Huang, X., Yang, N., Fiore, V. F., Barker, T. H., Sun, Y., Morris, S. W., et al. (2012). Matrix stiffness-induced myofibroblast differentiation is mediated by intrinsic mechanotransduction. *Am. J. Respir. Cell Mol. Biol.* 47 (3), 340–348. doi:10.1165/rcmb.2012-0050OC

Humphrey, J. D., Dufresne, E. R., and Schwartz, M. A. (2014). Mechanotransduction and extracellular matrix homeostasis. *Nat. Rev. Mol. Cell Biol.* 15 (12), 802–812. doi:10.1038/nrm3896

Ikenaga, N., Peng, Z. W., Vaid, K. A., Liu, S. B., Yoshida, S., Sverdlov, D. Y., et al. (2017). Selective targeting of lysyl oxidase-like 2 (LOXL2) suppresses hepatic fibrosis progression and accelerates its reversal. *Gut* 66 (9), 1697–1708. doi:10.1136/gutjnl-2016-312473

Jun, J. I., and Lau, L. F. (2017). CCN2 induces cellular senescence in fibroblasts. *J. Cell Commun. Signal.* 11 (1), 15–23. doi:10.1007/s12079-016-0359-1

Kim, B., Kim, H., Jung, S., Moon, A., Noh, D. Y., Lee, Z. H., et al. (2020). A CTGF-RUNX2-RANKL Axis in breast and prostate cancer cells promotes tumor progression in bone. *J. Bone Min. Res.* 35 (1), 155–166. doi:10.1002/jbmr.3869

Leong, S. S., Wong, J. H. D., Md Shah, M. N., Vijayananthan, A., Jalalonmuhali, M., Chow, T. K., et al. (2021). Shear wave elastography accurately detects chronic changes in renal histopathology. *Nephrology* 26 (1), 38–45. doi:10.1111/nep.13805

Li, B., and Wang, J. H. (2011). Fibroblasts and myofibroblasts in wound healing: Force generation and measurement. *J. Tissue Viability* 20 (4), 108–120. doi:10.1016/j.jtv.2009.11.004

Lipson, K. E., Wong, C., Teng, Y., and Spong, S. (2012). CTGF is a central mediator of tissue remodeling and fibrosis and its inhibition can reverse the process of fibrosis. *Fibrogenes. Tissue Repair* 5 (1), S24. doi:10.1186/1755-1536-5-S1-S24

Liu, F., Lagares, D., Choi, K. M., Stopfer, L., Marinkovic, A., Vrbanac, V., et al. (2015). Mechanosignaling through YAP and TAZ drives fibroblast activation and fibrosis. *Am. J. Physiol. Lung Cell. Mol. Physiol.* 308 (4), L344–L357. doi:10.1152/ajplung.00300.2014

Liu, F., Mih, J. D., Shea, B. S., Kho, A. T., Sharif, A. S., Tager, A. M., et al. (2010). Feedback amplification of fibrosis through matrix stiffening and COX-2 suppression. *J. Cell Biol.* 190 (4), 693–706. doi:10.1083/jcb.201004082

Liu, G., Cooley, M. A., Jarnicki, A. G., Borghuis, T., Nair, P. M., Tjin, G., et al. (2019). Fibulin-1c regulates transforming growth factor-beta activation in pulmonary tissue fibrosis. *JCI Insight* 5 (16), 124529. doi:10.1172/jci.insight.124529

McKinnon, D. D., Domaille, D. W., Cha, J. N., and Anseth, K. S. (2014). Biophysically defined and cytocompatible covalently adaptable networks as viscoelastic 3D cell culture systems. *Adv. Mat.* 26 (6), 865–872. doi:10.1002/adma.201303680

Mogi, M., and Kondo, A. (2010). ELISA for RANKL-OPG complex in mouse sera. *J. Immunoass. Immunochem.* 31 (2), 103–110. doi:10.1080/15321811003617305

Nguyen, X. X., Nishimoto, T., Takihara, T., Mlakar, L., Bradshaw, A. D., and Feghali-Bostwick, C. (2021). Lysyl oxidase directly contributes to extracellular matrix production and fibrosis in systemic sclerosis. *Am. J. Physiol. Lung Cell. Mol. Physiol.* 320 (1), L29–L40. doi:10.1152/ajplung.00173.2020

Noordhoek, J. A., Postma, D. S., Chong, L. L., Menkema, L., Kauffman, H. F., Timens, W., et al. (2005). Different modulation of decorin production by lung fibroblasts from patients with mild and severe emphysema. *COPD* 2 (1), 17–25. doi:10.1081/copd-200050678

Paapstel, K., Zilmer, M., Eha, J., Tootsi, K., Piir, A., and Kals, J. (2016). Association between fibulin-1 and aortic augmentation index in male patients with peripheral arterial disease. *Eur. J. Vasc. Endovasc. Surg.* 51 (1), 76–82. doi:10.1016/j.ejvs.2015.09.004

Parker, M. W., Rossi, D., Peterson, M., Smith, K., Sikstrom, K., White, E. S., et al. (2014). Fibrotic extracellular matrix activates a profibrotic positive feedback loop. *J. Clin. Invest.* 124 (4), 1622–1635. doi:10.1172/JCI71386

Petzold, G., Hofer, J., Ellenrieder, V., Neesse, A., and Kunsch, S. (2019). Liver stiffness measured by 2-dimensional shear wave elastography: Prospective evaluation of healthy volunteers and patients with liver cirrhosis. *J. Ultrasound Med.* 38 (7), 1769–1777. doi:10.1002/jum.14866

Piersma, B., Bank, R. A., and Boersema, M. (2015). Signaling in fibrosis: TGF-beta, WNT, and YAP/TAZ converge. *Front. Med.* 2, 59. doi:10.3389/fmed.2015.00059

Piersma, B., de Rond, S., Werker, P. M., Boo, S., Hinz, B., van Beuge, M. M., et al. (2015). YAP1 is a driver of myofibroblast differentiation in normal and diseased fibroblasts. *Am. J. Pathol.* 185 (12), 3326–3337. doi:10.1016/j.ajpath.2015.08.011

Pratsinis, H., Mavrogonatou, E., and Kletsas, D. (2019). Scarless wound healing: From development to senescence. *Adv. Drug Deliv. Rev.* 146, 325–343. doi:10.1016/j.addr.2018.04.011

Raghunathan, V. K., Morgan, J. T., Dreier, B., Reilly, C. M., Thomasy, S. M., Wood, J. A., et al. (2013). Role of substratum stiffness in modulating genes associated with extracellular matrix and mechanotransducers YAP and TAZ. *Invest. Ophthalmol. Vis. Sci.* 54 (1), 378–386. doi:10.1167/iovs.12-11007

Ravichandran, R., Islam, M. M., Alarcon, E. I., Samanta, A., Wang, S., Lundstrom, P., et al. (2016). Functionalised type-I collagen as a hydrogel building block for bio-orthogonal tissue engineering applications. *J. Mat. Chem. B* 4 (2), 318–326. doi:10.1039/c5tb02035b

Reinke, J. M., and Sorg, H. (2012). Wound repair and regeneration. *Eur. Surg. Res.* 49 (1), 35–43. doi:10.1159/000339613

Riser, B. L., Barnes, J. L., and Varani, J. (2015). Balanced regulation of the CCN family of matricellular proteins: A novel approach to the prevention and treatment of fibrosis and cancer. *J. Cell Commun. Signal.* 9 (4), 327–339. doi:10.1007/s12079-015-0309-3

Ruiz-Zapata, A. M., Heinz, A., Kerkhof, M. H., van de Westerlo-van Rijt, C., Schmelzer, C. E. H., Stoop, R., et al. (2020). Extracellular matrix stiffness and composition regulate the myofibroblast differentiation of vaginal fibroblasts. *Int. J. Mol. Sci.* 21 (13), E4762. doi:10.3390/ijms21134762

Sapir, L., and Tzlil, S. (2017). Talking over the extracellular matrix: How do cells communicate mechanically? *Semin. Cell Dev. Biol.* 71, 99–105. doi:10.1016/j.semcdb.2017.06.010

Schafer, M. J., White, T. A., Iijima, K., Haak, A. J., Ligresti, G., Atkinson, E. J., et al. (2017). Cellular senescence mediates fibrotic pulmonary disease. *Nat. Commun.* 8, 14532. doi:10.1038/ncomms14532

Schneider, C. A., Rasband, W. S., and Eliceiri, K. W. (2012). NIH image to ImageJ: 25 years of image analysis. *Nat. Methods* 9 (7), 671–675. doi:10.1038/nmeth.2089

Schuurman, W., Levett, P. A., Pot, M. W., van Weeren, P. R., Dhert, W. J., Hutmacher, D. W., et al. (2013). Gelatin-methacrylamide hydrogels as potential biomaterials for fabrication of tissue-engineered cartilage constructs. *Macromol. Biosci.* 13 (5), 551–561. doi:10.1002/mabi.201200471

Shirahama, H., Lee, B. H., Tan, L. P., and Cho, N. J. (2016). Precise tuning of facile one-pot gelatin methacryloyl (GelMA) Synthesis. *Sci. Rep.* 6, 31036. doi:10.1038/srep31036

Shome, D., von Woedtke, T., Riedel, K., and Masur, K. (2020). The HIPPO transducer YAP and its targets CTGF and Cyr61 drive a paracrine signalling in cold atmospheric plasma-mediated wound healing. *Oxid. Med. Cell. Longev.* 2020, 4910280. doi:10.1155/2020/4910280

Solon, J., Levental, I., Sengupta, K., Georges, P. C., and Janmey, P. A. (2007). Fibroblast adaptation and stiffness matching to soft elastic substrates. *Biophys. J.* 93 (12), 4453–4461. doi:10.1529/biophysj.106.101386

Stirling, D. R., Swain-Bowden, M. J., Lucas, A. M., Carpenter, A. E., Cimini, B. A., and Goodman, A. (2021). CellProfiler 4: Improvements in speed, utility and usability. *BMC Bioinforma.* 22 (1), 433. doi:10.1186/s12859-021-04344-9

Sun, M., Chi, G., Li, P., Lv, S., Xu, J., Xu, Z., et al. (2018). Effects of matrix stiffness on the morphology, adhesion, proliferation and osteogenic differentiation of mesenchymal stem cells. *Int. J. Med. Sci.* 15 (3), 257–268. doi:10.7150/ijms.21620

Tabatabaei, F., Moharamzadeh, K., and Tayebi, L. (2020). Fibroblast encapsulation in gelatin methacryloyl (GelMA) versus collagen hydrogel as substrates for oral mucosa tissue engineering. *J. Oral Biol. Craniofac. Res.* 10 (4), 573–577. doi:10.1016/j.jobcr.2020.08.015

Tjin, G., White, E. S., Faiz, A., Sicard, D., Tschumperlin, D. J., Mahar, A., et al. (2017). Correction: Lysyl oxidases regulate fibrillar collagen remodelling in idiopathic pulmonary fibrosis (doi: 10.1242/dmm.030114). *Dis. Model. Mech.* 10 (12), 1545. doi:10.1242/dmm.033191)

Totaro, A., Castellan, M., Battilana, G., Zanconato, F., Azzolin, L., Giulitti, S., et al. (2017). YAP/TAZ link cell mechanics to Notch signalling to control epidermal stem cell fate. *Nat. Commun.* 8 (1), 15206. doi:10.1038/ncomms15206

Tschumperlin, D. J., Ligresti, G., Hilscher, M. B., and Shah, V. H. (2018). Mechanosensing and fibrosis. *J. Clin. Invest.* 128 (1), 74–84. doi:10.1172/JCI93561

Uphoff, C. C., and Drexler, H. G. (2002). Detection of mycoplasma in leukemia-lymphoma cell lines using polymerase chain reaction. *Leukemia* 16 (2), 289–293. doi:10.1038/sj.leu.2402365

Valiente-Alandi, I., Potter, S. J., Salvador, A. M., Schafer, A. E., Schips, T., Carrillo-Salinas, F., et al. (2018). Inhibiting Fibronectin attenuates fibrosis and improves cardiac function in a model of heart failure. *Circulation* 138 (12), 1236–1252. doi:10.1161/CIRCULATIONAHA.118.034609

Verrecchia, F., and Mauviel, A. (2007). Transforming growth factor-beta and fibrosis. *World J. Gastroenterol.* 13 (22), 3056–3062. doi:10.3748/wjg.v13.i22.3056

Vial, C., Gutierrez, J., Santander, C., Cabrera, D., and Brandan, E. (2011). Decorin interacts with connective tissue growth factor (CTGF)/CCN2 by LRR12 inhibiting its biological activity. *J. Biol. Chem.* 286 (27), 24242–24252. doi:10.1074/jbc.M110.189365

Wang, B., Ke, W., Wang, K., Li, G., Ma, L., Lu, S., et al. (2021). Mechanosensitive ion channel Piezo1 activated by matrix stiffness regulates oxidative stress-induced senescence and apoptosis in human intervertebral disc degeneration. *Oxid. Med. Cell. Longev.* 2021, 8884922. doi:10.1155/2021/8884922

Wang, R., Yu, Z., Sunchu, B., Shoaf, J., Dang, I., Zhao, S., et al. (2017). Rapamycin inhibits the secretory phenotype of senescent cells by a Nrf2-independent mechanism. *Aging Cell* 16 (3), 564–574. doi:10.1111/acel.12587

Wang, Y., Michiels, T., Setroikromo, R., van Merkerk, R., Cool, R. H., and Quax, W. J. (2019). Creation of RANKL mutants with low affinity for decoy receptor OPG and their potential anti-fibrosis activity. *FEBS J.* 286 (18), 3582–3593. doi:10.1111/febs.14925

Waters, D. W., Blokland, K. E. C., Pathinayake, P. S., Wei, L., Schuliga, M., Jaffar, J., et al. (2019). STAT3 regulates the onset of oxidant-induced senescence in lung fibroblasts. *Am. J. Respir. Cell Mol. Biol.* 61 (1), 61–73. doi:10.1165/rcmb.2018-0328OC

Wershof, E., Park, D., Barry, D. J., Jenkins, R. P., Rullan, A., Wilkins, A., et al. (2021). A Fiji macro for quantifying pattern in extracellular matrix. *Life Sci. Alliance* 4 (3), e202000880. doi:10.26508/lsa.202000880

Westergren-Thorsson, G., Sime, P., Jordana, M., Gauldie, J., Sarnstrand, B., and Malmstrom, A. (2004). Lung fibroblast clones from normal and fibrotic subjects differ in hyaluronan and decorin production and rate of proliferation. *Int. J. Biochem. Cell Biol.* 36 (8), 1573–1584. doi:10.1016/j.biocel.2004.01.009

Wickert, L. E., Pomerenke, S., Mitchell, I., Masters, K. S., and Kreeger, P. K. (2016). Hierarchy of cellular decisions in collective behavior: Implications for wound healing. *Sci. Rep.* 6 (1), 20139. doi:10.1038/srep20139

Woldhuis, R. R., de Vries, M., Timens, W., van den Berge, M., Demaria, M., Oliver, B. G. G., et al. (2020). Link between increased cellular senescence and extracellular matrix changes in COPD. *Am. J. Physiol. Lung Cell. Mol. Physiol.* 319 (1), L48–L60. doi:10.1152/ajplung.00028.2020

Woldhuis, R. R., Heijink, I. H., van den Berge, M., Timens, W., Oliver, B. G. G., de Vries, M., et al. (2020). COPD-derived fibroblasts secrete higher levels of senescence-associated secretory phenotype proteins. *Thorax* 76, 508–511. thoraxjnl-2020. doi:10.1136/thoraxjnl-2020-215114

Yan, X., Xiong, X., and Chen, Y. G. (2018). Feedback regulation of TGF-beta signaling. *Acta Biochim. Biophys. Sin.* 50 (1), 37–50. doi:10.1093/abbs/gmx129

YasminMaskari, R. A., McEniery, C. M., Cleary, S. E., Li, Y., Siew, K., et al. (2018). The matrix proteins aggrecan and fibulin-1 play a key role in determining aortic stiffness. *Sci. Rep.* 8 (1), 8550. doi:10.1038/s41598-018-25851-5

Zhang, C., Zhu, H., Ren, X., Gao, B., Cheng, B., Liu, S., et al. (2021). Mechanics-driven nuclear localization of YAP can be reversed by N-cadherin ligation in mesenchymal stem cells. *Nat. Commun.* 12 (1), 6229. doi:10.1038/s41467-021-26454-x

Zhang, W., Ge, Y., Cheng, Q., Zhang, Q., Fang, L., and Zheng, J. (2018). Decorin is a pivotal effector in the extracellular matrix and tumour microenvironment. *Oncotarget* 9 (4), 5480–5491. doi:10.18632/oncotarget.23869

Zhao, B., Wei, X., Li, W., Udan, R. S., Yang, Q., Kim, J., et al. (2007). Inactivation of YAP oncoprotein by the Hippo pathway is involved in cell contact inhibition and tissue growth control. *Genes Dev.* 21 (21), 2747–2761. doi:10.1101/gad.1602907

Zhou, Y., Horowitz, J. C., Naba, A., Ambalavanan, N., Atabai, K., Balestrini, J., et al. (2018). Extracellular matrix in lung development, homeostasis and disease. *Matrix Biol.* 73, 77–104. doi:10.1016/j.matbio.2018.03.005

Zhou, Z., Qu, J., He, L., Zhu, Y., Yang, S. Z., Zhang, F., et al. (2020). Stiff matrix instigates type I collagen biogenesis by mammalian cleavage factor I complex-mediated alternative polyadenylation. *JCI Insight* 5 (3), 133972. doi:10.1172/jci.insight.133972

Zhu, M., Wang, Y., Ferracci, G., Zheng, J., Cho, N-J., and Lee, B. H. (2019). Gelatin methacryloyl and its hydrogels with an exceptional degre of controllability and batch-to-batch consistency. *Sci. Rep.* 9 (1), 6863. doi:10.1038/s41598-019-42186-x